Performance of a Faraday Rare Gas Alkali MHD Generator

G. BREDERLOW,* K. J. WITTE,* AND H. ZINKO†
Max-Planck-Institut für Plasmaphysik, Garching, F.R. Germany

The performance of the IPP rare gas alkali MHD generator was theoretically and experimentally investigated. The open-circuit Faraday voltage, the short-circuit Hall voltage, and the load characteristic were measured at different segmentation ratios s/h and various magnetic field strengths. Furthermore, the current streamline pattern in the generator duct was determined from the equipotential lines measured by means of a movable probe. From these measurements it could be concluded that the generator is practically free of any leakage currents and internal plasma short-circuits. This conclusion was further supported by the reasonably good agreement between theory and experiment regarding the current voltage characteristic of the generator. In the calculation allowance was made for the influence of ionization instabilities, segmentation effects, and voltage drops at the electrode, but mechanisms producing leakage currents or internal plasma short-circuits were not considered.

1. Introduction

IN rare gas alkali MHD generators the electron density and hence the electrical conductivity attain equilibrium in accordance with the electron temperature elevation. This "nonequilibrium ionization" in conjunction with the fact that the electron temperature elevation in the generator may show strong local variations and occurs in a medium flowing at high velocity through the generator duct gives rise to a number of complications which are not so pronounced in the case of an equilibrium generator or not even present there. The most important ones are: elongation of the current paths due to relaxation and convection effects particularly pronounced at the generator entrance, inhomogeneities in the current density distribution produced by the electrode configuration, axial leakage currents and ionization instabilities. All of these phenomena impair the performance of the generator. It is therefore necessary to investigate them, and if possible, lessen their influence.

The performance of "nonequilibrium" MHD generators has already been investigated in a variety of test rigs. It was possible to achieve high power densities and electron temperature elevations in short-time MHD generator systems[1,2] with operating times of up to a few milliseconds. The test rigs working in continuous operation[3,4] involved technical problems which prevented the theoretically predicted power output from being attained. Better, but still not quite the ideal values of the power density and electron temperature elevation were obtained in the "blow-down facilities."[5-7] Whereas this deviation is accounted for in Ref. 5 by assuming external leakages strictly associated with the duct technology, it is ascribed in Refs. 6 and 7 to the presence of highly conducting layers along the electrode walls which impair the generator performance.

This paper reports investigations on a generator working in continuous operation. These were concerned not only with the measurement of the Faraday voltage across the duct, the Hall voltage between the electrodes, and the current flowing through one electrode pair, but also with the local distributions of the various plasma parameters, viz., the potential and current density distributions, the velocity profile, and the electron and gas temperatures. The dependence of the current-voltage characteristics and the power density on individual generator parameters was determined. Furthermore, the most favorable possible electrode configuration was chosen, effective preionization was performed, and leakage currents were suppressed in an attempt to achieve optimum conditions.

2. Experimental Conditions and Apparatus

The measurements are made in a potassium-seeded argon plasma under controlled conditions of purity, temperature, and composition. The gas temperature is up to 2000°K, the seed concentration 0.14%, and the gas pressure about 1.3 bar. The maximum mean flow velocity obtained in the generator duct with 20×30 mm^2 cross section is 425 mps, ($M = 0.52$) at a flow rate of 80 g argon/sec.

In the test rig, designed as a closed loop, the gas is heated by a 200 kw arc heater and mixed with the potassium vapor in the mixing chamber. The mixture then flows through the MHD generator to a heat exchanger, where it is cooled down. The potassium is then removed by a glass-wool filter and the pure argon is returned to a compressor to be recycled. In order to maintain safe and reliable operation of the equipment, the gas loop was maintained with automatic control facilities. A detailed description of the equipment used is given in Ref. 8.

The generator duct housing is constructed to allow maximum freedom of choice of diagnostic methods and duct geometries combined with ease of assembly and disassembly. Air core magnetic field coils were chosen to provide free access for optical diagnostics. They provide a maximum magnetic field of 5.0 tesla with 5% nonuniformity over a length of 300 mm. The duct itself has a cross section of 20×30 mm^2 and is 100 mm long. It is made from Al_2O_3 blocks fitted flush together.

The geometry of the duct is shown in Fig. 1. Up to 33 circular

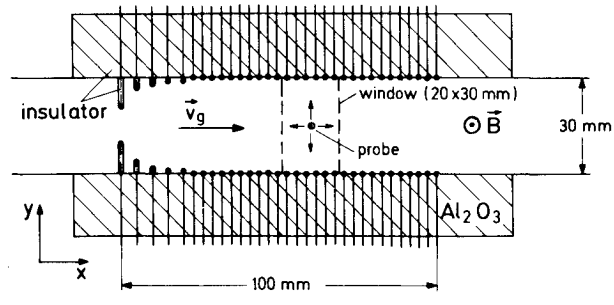

Fig. 1 Diagram of the MHD generator duct.

Received April 23, 1973; revision received October 29, 1973. This work was undertaken as part of the joint research program between the Max-Planck-Institut für Plasmaphysik and Euratom. The authors wish to express their gratitude to Mr. Borde, Mr. Hartmann, and Mr. Geisreiter for the construction of the apparatus and the assistance in the experiments.

Index categories: Plasma Dynamics and MHD; Electrical Power Generation Research.

* Research Scientists.

† Research Scientist; now at Aktiebolaget Atomenergi, Studsvik Nyköping, Schweden.

electrodes 1 mm in diameter with periodicity intervals of 2, 3, and 6 mm were used. In the entrance region of the duct five pairs of electrodes were placed in the gas flow. The spacing between opposite electrodes was gradually increased from 8 mm at the duct entrance to the normal spacing of 30 mm. This electrode arrangement proved to ensure the most effective preionization by applying external electric fields in the direction of the $v \times B$ e.m.f.

In order to prevent shortening of the Hall field by leakage currents, the different parts of the housing of the system were carefully insulated from one another, from the plasma, and from the ground (for details see Ref. 8).

3. Diagnostic Devices and Methods

In order to determine the spatial distribution of the plasma parameters in the center region of the generator duct, movable side walls are used in the corresponding region of the channel (dashed region in Fig. 1). Each side wall has a hole which can be moved in the x-y plane. Through this hole a thermocouple, a pitot tube or an electrostatic probe can be inserted.

In the case of spectroscopic measurements on the potassium resonance lines pure argon is blown through the holes in the side walls in order to prevent selfabsorption by displacing the potassium in the colder boundary layer.[8] The electron temperature is measured by the line reversal method in the wing of one of the potassium resonance lines. The investigations described in Ref. 9 indicate that in the argon-potassium plasma used the population temperature investigated by this method is practically equal to the electron temperature. The gas temperature is determined with tungsten-rhenium thermocouples in the region of the movable side wall in the y and z directions. The wall temperatures in the duct were also checked with thermocouples. (The calibration of the thermocouples is described in Refs. 26 and 8.)

The velocity in the generator duct is measured by inserting a pitot probe through one movable side wall. The probe consists of a 1 mm alumina tube with a radial hole 0.5 mm in diam, which was used for measuring the stagnation pressure. The static pressure is measured at the duct wall in the same y-z plane in which the pitot tube was moved. Evaluation of the velocity profile calls for a knowledge of the gas density, i.e., the distribution of the gas temperature in the generator cross section. To measure the gas temperature, the pitot tube was replaced by a thermocouple which could be shifted in both the y and z directions.

To measure the potential distribution, a cylindrical probe, 0.5 mm in diam was inserted in the duct through the hole of one movable side wall. The potential distribution was determined by measuring the potential between the probe and one of the duct electrodes at high impedance as functions of space. As only the potential differences occurring in the plasma are of interest here, the negative potential difference always present between the probe and the surrounding plasma is only important in so far as it varies strongly in space. According to the estimates made in Ref. 10 the potential difference between a cold probe and the plasma under the given conditions is in the region of 1 v. This difference can increase near the wall, where there are strong gradients of the electron temperature and the electron and ion densities. With the hot probe used here, however, this potential difference decreases under the influence of the electron emission and magnetic field. These effects cannot, however, be exactly calculated. In the generator plasma investigated the potential differences between the probe and plasma were so small compared with those measured that they practically did not impair the experimental accuracy.

4. Theory

In order to understand and interpret the experimental results properly, it is useful to compare them with some theoretical calculations. The model which we propose to explain the generator performance will be discussed in detail in this section.

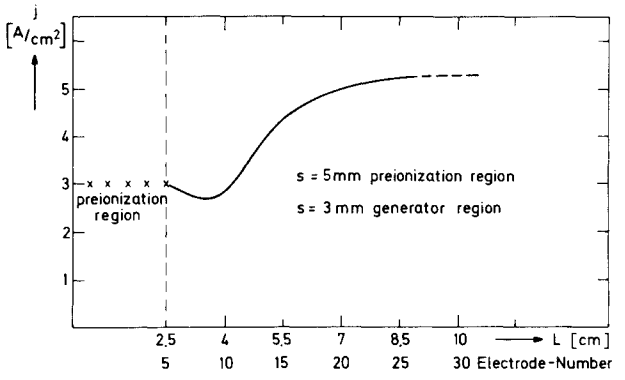

Fig. 2 Short-circuit current density along the generator duct. $s/h = 0.1$; $B = 4$ tesla; $V = 420$ mps; $T_g = 2000°K$; $p = 1.28$ bar.

In our analysis neither leakage currents due to insufficient wall insulation or ground loops nor conducting layers at the electrode walls as described in Ref. 6 will be taken into account. We also assume that the ionization instability is always present and that the plasma is everywhere turbulent. Furthermore, only that part of the generator duct will be considered where periodic conditions are achieved, that is, where the bulk properties of the plasma do not change any more in the direction of the duct axis. Such a situation is given in the last section of the duct behind the 20th electrode pair (see Fig. 2). Since the electric energy generated in the duct is small compared with the thermal energy of the gas flow because of the short duct length, we may also neglect the variation of the gasdynamic quantities such as T_g and p along the duct axis and treat them as constants.

It is assumed that the turbulence of the plasma is such that Saha's equation is still valid at any point in space and at every moment. Because we are more interested in instantaneous space averages, denoted by pointed brackets $\langle \ldots \rangle$, than in the local behavior of the plasma, we write

$$\langle N_e \rangle \simeq -\tfrac{1}{2} f_s(\langle T_e \rangle) + [\tfrac{1}{4} f_s^2(\langle T_e \rangle) + N_k^0 f_s(\langle T_e \rangle)]^{1/2} \tag{1}$$

where

$$f_s(T_e) = \left(\frac{m_e k T_e}{2\pi\hbar^2}\right)^{3/2} \exp\left(-\frac{\varepsilon_i}{kT_e}\right) \tag{2}$$

If the volume over which the averaging process is performed is large compared with the third power of a characteristic length scale of the plasma (a few millimeters in our case) all the average values will be practically constant and equal to the time average.

Strictly speaking, Eq. (1) is only approximately valid because the contributions arising from the fluctuations in T_e have been neglected. This, however, is permissible because they are very small.[11]

The next equation needed for the calculation of the generator performance is the averaged Ohm's law which we write in the form

$$\langle j_y \rangle = \frac{\sigma_{\text{eff}} vB}{1 + g\beta_{\text{eff}}} \left(-1 + \frac{U}{vBh}\right) \tag{3a}$$

$$\beta_{\text{eff}} = \frac{\beta_{\text{eff}} + g}{1 - g\beta_{\text{app}}} \tag{3b}$$

where we have used the definitions

$$\beta_{\text{app}} = \langle E_x \rangle / (\langle E_y \rangle - vB) \tag{4}$$

$$U = h\langle E_y \rangle \tag{5}$$

$$g = -\langle J_x \rangle / \langle J_y \rangle \tag{6}$$

β_{app} is the apparent Hall parameter which can be derived from probe measurements, U is the voltage drop across the generator duct, and h the channel height.

The quantity $\sigma_{\text{eff}}/(1 + g\beta_{\text{eff}})$ can be considered as a measure of the internal resistance of the generator, which depends not only

on the effective plasma properties σ_{eff} and β_{eff}, but also on the geometrical configuration of the electrodes, i.e., the size of segmentation used. This dependence is accounted for by the factor g. Physically, it can be understood as a measure of the elongation of the current path from the anode to the cathode compared with an ideal generator, where the x-component of the current density vector is everywhere zero. With the results obtained in Refs. 12–14 it can be shown that for a nonequilibrium generator g can be approximated by

$$g = 1.4s/h \tag{7}$$

with some uncertainty regarding the preciseness of the factor 1.4. The next equation needed is the energy equation of the free electrons

$$\frac{\langle J\rangle^2}{\sigma_{\text{eff}}} = \langle \dot{E}_{el}\rangle + \langle \dot{E}_R\rangle \tag{8}$$

where $\langle \dot{E}_{el}\rangle$ and $\langle \dot{E}_R\rangle$ are the spatially averaged elastic and radiation losses. As can be shown by a detailed calculation, it is not necessary to take the contributions due to the fluctuations of N_e and T_e into account in determining $\langle \dot{E}_{el}\rangle$ and $\langle \dot{E}_R\rangle$. It is sufficient to approximate both quantities (the error is less than 3%) by

$$\langle \dot{E}_{el}\rangle = 3k(m_e/m_A)\langle \nu\rangle\langle N_e\rangle(\langle T_e\rangle - T_g) \tag{9}$$

$$\langle \dot{E}_R\rangle = 2\pi\frac{h+d}{hd}\{B_\lambda(\langle T_e\rangle) - B_\lambda(T_w)\}\Delta\lambda \tag{10}$$

Here $\langle \nu\rangle$ is the spatially averaged collision frequency and is given by

$$\langle \nu\rangle = \frac{4}{3}\left(\frac{8k\langle T_e\rangle}{\pi m_e}\right)^{1/2}\{N_A Q_{e-A}(\langle T_e\rangle) + (N_k^0 - \langle N_e\rangle)Q_{e-k} + \langle N_e\rangle Q_{e-I}(\langle T_e\rangle, \langle N_e\rangle)\} \tag{11}$$

where Q_{e-I} is the electron-ion cross section[15]

$$Q_{e-I}(\langle N_e\rangle, \langle T_e\rangle) = 2.22\times 10^{-10}\langle T_e\rangle^{-2}\times \ln\left\{1.24\times 10^7\left(\frac{\langle T_e\rangle^3}{\langle N_e\rangle}\right)^{1/2}\right\}[m^2] \tag{12}$$

with $\langle T_e\rangle$ in Kelvin and $\langle N_e\rangle$ in m^{-3}. The velocity averaged cross section Q_{e-A} is assumed to be a linear function of $\langle T_e\rangle$ in the range $2\times 10^3 \leqq \langle T_e\rangle \leqq 5\times 10^3$ according to ($\langle T_e\rangle$ in Kelvin)

$$Q_{e-A}(\langle T_e\rangle) = -0.32 + 0.46\cdot 10^{-3}\langle T_e\rangle \quad [\text{Å}^2] \tag{13}$$

The data necessary for deriving Eq. (13) were taken from Ref. 16. They were slightly changed ($\sim 15\%$) so as to give the best fit to the measurements of the laminar electrical conductivity carried out in Refs. 17 and 18. A constant value of 0.4×10^{-17} m^2 was chosen for the electron potassium cross section Q_{e-k}.[19] In Eqs. (11) and (12) the fluctuation correction has again been neglected because of its smallness. The formula for the radiation loss (10) was taken from Ref. 17. In this expression B_λ means the Planck's function and $\lambda = 0.7665$ μm is the center wavelength of one of the potassium resonance lines. T_w is the wall temperature and is related to the gas temperature by

$$T_w = T_g - 300^\circ \tag{14}$$

Finally, $\Delta\lambda$ (for details see Ref. 17) is given in the range $10^{-4} \leqq c \leqq 5\times 10^{-3}$ by

$$\Delta\lambda = 25 + 10^4 c \quad [\text{Å}] \tag{15}$$

where c is the seed concentration. The last equation needed refers to the effective electrical conductivity. Several suggestions have been made how to calculate σ_{eff} as a function of the spatially averaged plasma properties $\langle\sigma\rangle$, $\langle\beta\rangle$ or $\langle j\rangle$. By means of a quasi-linear analysis of plane ionization waves of arbitrary shape it was found in Ref. 20 that

$$\frac{\sigma_{\text{eff}}}{\langle\sigma\rangle} = \left(\frac{\sigma_N^2 + \beta_{\text{crit}}^2}{\sigma_N^2 + \langle\beta\rangle^2}\right)^{1/2} \tag{16}$$

In Ref. 21 plane square waves with zero phase shift are considered, yielding

$$\frac{\sigma_{\text{eff}}}{\langle\sigma\rangle} = \frac{\sigma_N + (\sigma_N^2 + \beta_{\text{crit}}^2)^{1/2}}{\sigma_N + (\sigma_N^2 + \langle\beta\rangle^2)^{1/2}} \tag{17}$$

Both relations should hold for a plasma which has just started to be unstable. For high values of the Hall parameter where the fluctuation spectrum tends to become turbulent Eq. (16) should yield a lower limit to the reduction in conductivity. $\langle\sigma\rangle$ and $\langle\beta\rangle$ are the spatially averaged electrical conductivity and Hall parameter and can be approximately determined from

$$\langle\sigma\rangle = \sigma(\langle N_e\rangle, \langle T_e\rangle) = \frac{e^2\langle N_e\rangle}{m_e\langle\nu\rangle} f(\langle T_e\rangle, \langle\beta\rangle) \tag{18}$$

and

$$\langle\beta\rangle = \beta(\langle N_e\rangle, \langle T_e\rangle) = eB/m_e\langle\nu\rangle \tag{19}$$

The calculation of $\langle\sigma\rangle$ had to allow for the fact that in a plasma with collision cross sections dependent on the electron energy the value of $\langle\sigma\rangle$ decreases if a transverse magnetic field is applied. This influence is accounted for by the factor f, which was taken from Ref. 22. As before, the fluctuation correction has again been neglected because the error is small (less than 3%). σ_N is a logarithmic derivative and is given by

$$\sigma_N = \left.\frac{d\ln\sigma}{d\ln N_e}\right|_{\substack{N_e=\langle N_e\rangle \\ T_e=\langle T_e\rangle}} \tag{20}$$

β_{crit} is the critical Hall parameter indicating the onset of the ionization instability and can be obtained from

$$\beta_{\text{crit}} = (\dot{E}_{el,N}^2 - \sigma_N^2)^{1/2} \tag{21}$$

where

$$\dot{E}_{el,N} = \left.\frac{d\ln\dot{E}_{el}}{d\ln N_e}\right|_{\substack{N_e=\langle N_e\rangle \\ T_e=\langle T_e\rangle}} \tag{22}$$

For a highly turbulent plasma ($\langle\beta\rangle \gg \beta_{\text{crit}}$) consisting of "two phases," whereby the volumes occupied by the phases are equal and their locations are random, an exact calculation of the effective conductivity was made in Ref. 23, yielding

$$\sigma_{\text{eff}}/\langle\sigma\rangle = (\beta_{\text{eff}}/\langle\beta\rangle) \tag{23}$$

β_{eff} is not constant, but depends on the Hall parameter $\langle\beta\rangle$ and the mean square value $(\langle\tilde{\sigma}^2\rangle)^{1/2}$ of the fluctuations in σ. In order to check the applicability of Eq. (23) for a calculation of the generator performance, β_{eff} has to be known with an accuracy of less than 5% (see Fig. 4). Since $\langle\tilde{\sigma}\rangle$ has to be taken from measurements and such precision cannot be expected there, we have made no attempt to investigate further the model proposed in Ref. 23. Besides the two relations (16) and (17), we checked a third formula for σ_{eff} which can formally be derived from Eq. (16) by assuming that $\sigma_N^2 \ll \beta_{\text{crit}}^2, \langle\beta\rangle^2$ (Coulomb collision dominated plasma; such a situation is almost reached in the neighborhood of the short-circuit case), which leads to

$$\sigma_{\text{eff}}/\langle\sigma\rangle = \beta_{\text{crit}}/\langle\beta\rangle \tag{24}$$

However, Eq. (24) can also be considered as a semiempirical description of the dependence of σ_{eff} on the spatially averaged plasma properties valid both for a neutral collision and a Coulomb collision dominated plasma. In all the formulas for σ_{eff} [Eqs. (16, 17, 23, and 24)] it is implicitly assumed that at the same current density the electron temperature or electron density in a turbulent plasma is expected to be much higher than in a laminar one. The experimental results obtained in Refs. 21, 24, 25 confirm this conclusion. However, no appreciable increase in the ohmic heating of the electrons in a turbulent plasma had been observed in Ref. 18. This weak elevation of the electron temperature is probably due to the fact that in the longitudinal discharge the current density profile in the $v\times B$ direction is changed by the $j\times B$ forces and therefore the radiation measurements made in the center region of the duct may not be representative for the average electron temperature of the plasma. In addition, the small surface to volume ratio in Ref. 18 increases the influence of the radiation losses.

In order to find out which of the formulas for σ_{eff} given previously describes the dependence of the effective conductivity on the current density and magnetic induction best and should therefore be used for the calculation of the generator performance, we compared them with the experimental results for

σ_{eff} obtained in Ref. 18 in the $\langle j \rangle$ and B ranges investigated ($\langle j \rangle = 0.1$–$5\ A/cm^2$, $B = 0$–1.5 tesla). Formulas (16) and (24) fit the experimental effective conductivity data quite well. Formula (17) predicts values which are slightly better than the experimental one. For $B > 1\ T$ formula (23)—if one takes the values for β_{eff} given in Ref. 18—also reproduces the measurements reasonably well. From this comparison we have to conclude that none of these formulas can be ruled out definitely except (23) because β_{eff} is not known precisely enough in the generator duct, and that they can all be used for the calculation of the current-voltage characteristic of the generator which has been done with the assumption of a constant β_{eff} taken from measurements.

In order to compare the theoretically determined performance of the generator with that measured, it is necessary to allow for the energy which is dissipated in the anode and cathode falls. These electrode regions have the same function as an external load resistance and owing to the relatively small duct dimensions in our test rig the energy converted there is mostly of the order of that delivered to the external load resistance. The length over which the voltage drop at the electrodes occurs is very small, less than 1mm, so that within the approximation of our calculation we do not have to correct the duct height by treating the anode and cathode falls as additional external load resistances. We may therefore write for the voltage U across the generator duct

$$U = U_L + U_E \tag{25}$$

where U_L is the voltage drop which can be measured at the real load resistance and U_E is the sum of the voltage drop at the anode and cathode. U_E is shown in Fig. 3 as a function of the current I_y flowing through one electrode pair. This curve was determined by probe measurements.

In calculating the current I_y per electrode pair from the current density $\langle j_y \rangle$ according to the relation

$$I_y = \langle j_y \rangle sd\,0.9 \tag{26}$$

we have assumed that not the whole area sd is effective, but only 90% of it. This estimate is based on the experimental results obtained in Ref. 17. Physically, Eq. (26) reflects the fact that the plasma properties are not constant along the magnetic field lines, but exhibit a profile.

Finally, it should be emphasized that this calculation of the generator performance contains two uncertainties. The first refers to the g-factor, i.e., the influence of the electrode geometry on the internal resistance of the generator, and the second to the effective electrical conductivity, which is theoretically known only for some special cases that are usually only approximately realized in the conditions prevailing in an MHD generator. From the measurements, however, it is possible to estimate the degree of uncertainty in these two cases and, more especially, to decide which of the formulas for the effective electrical conductivity [Eqs. (16, 17, and 24)] are appropriate for calculating the generator performance.

5. Results

5.1 Temperature and Flow Velocity Profiles and Open-Circuit Voltages

The flow and temperature distributions in the measuring duct showed turbulent profiles ($R_e \simeq 3 \times 10^4$). The normalized temperature and velocity profiles measured in the y-direction at zero magnetic field did practically coincide.

With a magnetic field applied one would expect under open-circuit conditions a flattening of the velocity profile. But the measurements revealed only a 3%–5% reduction of the flow velocity in the center of the duct and a corresponding reduction of the boundary-layer thickness at a Hartmann number of about 100. The calculation of this number is based on the core flow conductivity at a magnetic induction of 1 tesla. The relatively small influence of the $j \times B$ forces on the velocity profiles is due to the following facts. First, the Hartmann number in the vicinity of the walls corresponding to the temperature and hence conductivity profile is much less than in the central regions of the duct. Second, the measuring region is located so close to the entrance of the MHD duct that a fully MHD profile cannot be expected. More information about this phenomenon and further measurements of the velocity and temperature profiles at various Hartmann numbers are given in Ref. 26.

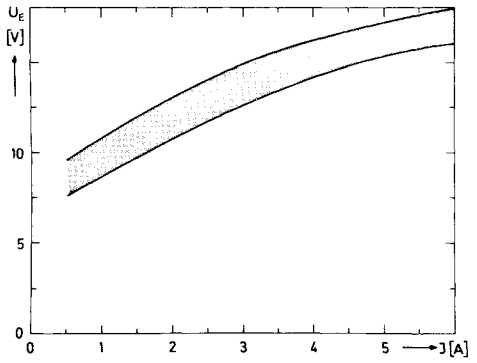

Fig. 3 Sum of the cathode and anode drops as a function of the current per electrode pair. Region of reproducibility is denoted by the upper and lower curves. $V = 420$ mps; $T_g = 2000°K$; $p = 1.3$ bar.

By replacing the pitot tube by an electrostatic probe and measuring the voltage between the probes and one of the electrodes the slope of the induced $v \times B$ e.m.f. could be determined. Within the accuracy of our measurements of $\pm 5\%$ the velocity profile in the y-direction thus obtained was in good agreement with the pitot tube measurements.

The open-circuit voltage measured between one electrode pair may be up to 20% higher than the value based on the averaged flow velocity. This result indicates that there are only very small circular currents in the y-z plane, although there are strong local differences in the $v \times B$ e.m.f.s. This result is also in agreement with the fact that the velocity profile is only very slightly changed by the $j \times B$ forces. A detailed description of these phenomena is afforded by the calculations in Ref. 27. Under normal conditions the open-circuit voltage was always a linear function of the magnetic induction. There were, however, deviations from linearity, and the voltage was also lower than theoretically predicted when the insulation of the generator duct and, in particular, that of the side walls was insufficient. In this case it was also possible to measure a Hall voltage between the individual electrode pairs, which indicates the presence of eddy currents that flow in the plasma along the side walls in the $v \times B$ direction and back. This inadequate insulation occurred when the generator duct was in operation for longer than a total of 20–30 hr. The insulating properties of the Al_2O_3 used were apparently impaired in the hot rare gas alkali atmosphere. It was therefore found advisable to check the insulation state of the generator duct before commencement of a test series by measuring the open-circuit voltage.

5.2 Short-Circuit Current Density

To obtain the theoretically predicted short-circuit current density in the generator duct used here, it is necessary to have good insulation of the duct and the entire test rig. The insulation conditions of the test rig therefore had to be checked where possible. One method which essentially covers the y-direction in the duct has already been described in Sec. 5.1. Furthermore, for the generator to work under load conditions it is necessary to have good insulation in the x-direction. This can easily be checked by connecting the initial and final electrode pairs with a variable resistance R_α. If the rig is properly insulated, the value of the resistance R_α should have a marked influence on the short-circuit current density, even for high values of R_α. In our case the threshold value of R_α was about 1 kΩ; variations of R_α in the region of $\geqq 1$ kΩ no longer had any effect on the short-circuit current density.

As the ducts used here were relatively short, sufficient pre-

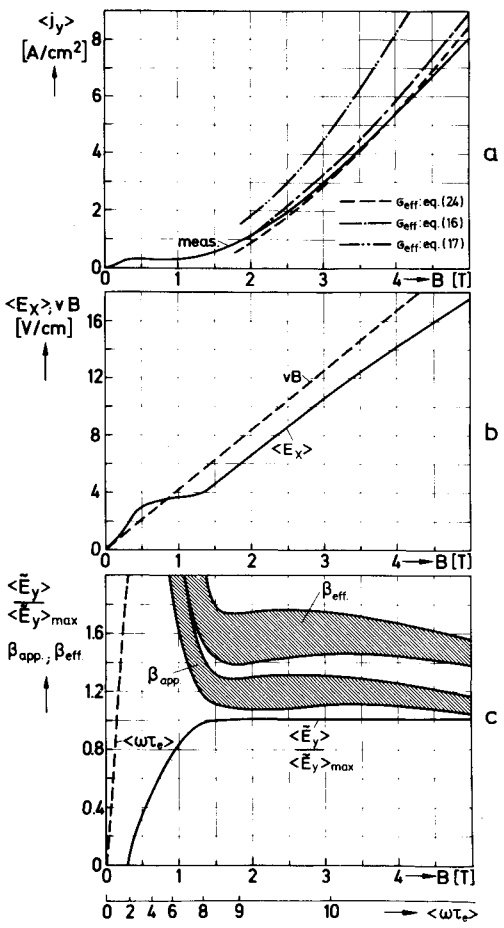

Fig. 4 Short-circuit current density (a); short-circuit Hall and open-circuit Faraday field strengths (b); apparent and effective Hall parameters and normalized amplitudes of the electric field fluctuation under short-circuit conditions (c) as a function of the magnetic induction. (The $\langle\omega\tau_e\rangle$ abscissa is valid for all curves except vB.) $s/h = 0.1$; $V = 415$ mps; $T_g = 2000°K$; $p = 1.3$ bar.

ionization was needed in addition to good insulation. The reason was that under the given conditions the relaxation lengths may be in the region of a few cm. In the region of the relaxation length the performance of the generator is impaired since the equilibrium carrier density has not yet been attained. Because the carrier density increases in the flow direction the current lines are swept downstream and therefore the current paths become longer. This fact has already been observed experimentally[28] and has been confirmed by numerical calculation.[29]

In the relaxation region the available $v \times B$ e.m.f. has to drive the current flow along highly elongated current paths. This means that in the entrance relaxation region the internal resistance of the generator is higher than further downstream where periodic conditions are reached. Consequently, the current density and hence the elevation of the electron temperature and the ionization rate is low. This leads to relaxation lengths which in small experimental generators may be larger than the duct lengths.

To obtain the shortest possible relaxation lengths in the experiment, the field strength E_y^* in the entrance region of the generator duct was increased by applying separate additional external electric fields to the five entrance electrode pairs in the direction of the induced e.m.f. A special electrode configuration ensured that the current flows through the plasma by the shortest possible path without strong bulging of the current lines in the downstream direction. Periodic conditions were then obtained 6 cm downstream from the duct entrance, as shown in Fig. 2. In this figure the short-circuit current density is plotted as a function of the number of electrode pairs. An external electric field was individually applied to the first five entrance electrode pairs, whereby a total power of 100 w was fed into the plasma. At the first electrode pairs after the preionization region the induced current density was smaller than in the preionization region. As calculations of the ionization relaxation lengths show, this is due to the fact that periodic conditions could not yet be obtained here. The current paths therefore bulge downstream and the induced e.m.f. has to produce the current flux along elongated streamlines. Behind the 20th electrode pair periodic conditions were, however, practically reached.

The variation of the short-circuit current density is given in Fig. 4a as a function of the magnetic induction. The measurement was made at the 22nd electrode pair, where periodic conditions were already present. The measuring accuracy was $\pm 6\%$. The values given here and in the following curves are time and spatially averaged values. The respective Hall parameters calculated are given on the abscissa. Three sections of the curve can be distinguished. First the current density rises linearly to values of $\langle j\rangle = 0.3$ amp/cm^2 ($B = 0.3$ T), then remains approximately constant up to $B = 1.3$ T and finally resumes its roughly linear increase.

To explain this behavior, it was also necessary to plot the curves for the Hall field strength inside the duct $\langle E_x\rangle$ (Fig. 4b), the Hall parameter β_{app} (Fig. 4c) and the relative field fluctuations due to ionization instabilities (Fig. 4c).

To calculate β_{app}, not only has $\langle E_x\rangle$ to be determined, but also $v \times B$ and $\langle E_y\rangle$. The $v \times B$ e.m.f. is plotted in Fig. 4b as a function of the magnetic induction. $\langle E_y\rangle$ is obtained from the sum of the cathode and anode drops prevailing at the respective short-circuit current strengths.

This sum is plotted in Fig. 3 as a function of the current strength. This value was determined by probe measurements. In agreement with the measurements in Ref. 10 it was found that both the cathode and anode drops depend practically only on the current per electrode pair, and not on the magnetic field or segmentation. The main voltage drop occurred at the cathode. The anode drop was always in the region of 1–2 v. The measuring method allows the voltage drop at the electrodes to be determined with an accuracy of ± 0.5 v. Since, however, the voltage drops were not exactly reproducible throughout the series of measurements, the fluctuation range is given in Fig. 3.

The curves for the short-circuit current density, the Hall parameter and the onset of field fluctuations (Fig. 4a–c) show that beyond $\langle\beta\rangle = 4$ the generator performance is governed by ionization instabilities. This relatively high value of the critical Hall parameter is due to the low short-circuit current density. Contrary to expectation, the short-circuit current density increases linearly with the magnetic induction in the stable region from 0 to 0.3 tesla. This linear rise is due to the fact that the electrical conductivity here is constant. The reason for this is that the electron density in the low current density range is higher than is in keeping with the local electron temperature. This excess carrier density is caused by electrons which are dragged from the plasma jet into the measuring duct by the flow.[17]

In the unstable region the short-circuit current density is approximately constant (up to 1.3 tesla) and then undergoes a slight increase. This behavior of the short-circuit current density is due to the fact that σ_{eff} initially takes a pronounced drop with increasing magnetic field at the onset of ionization instabilities and then decreases again less steeply. The region of strong decrease ($\sigma_{eff} \sim \text{const}/B$) coincides with that of constant current density.

At magnetic inductions exceeding 1.3 tesla the short-circuit current density then increases. This is also partly due to the fact that the importance of the voltage drops at the electrodes decreases with increasing $v \times B$ e.m.f.

In the region from 0 to 1.3 tesla it is not possible at first to obtain any reliable experimental results on the behavior of the Hall parameter $\beta_{app} = [\langle E_x\rangle/(v \times B - \langle E_y\rangle)]$. This is because the difference $v \times B - \langle E_y\rangle$ cannot be determined very accurately in this region since the two quantities are approximately equal

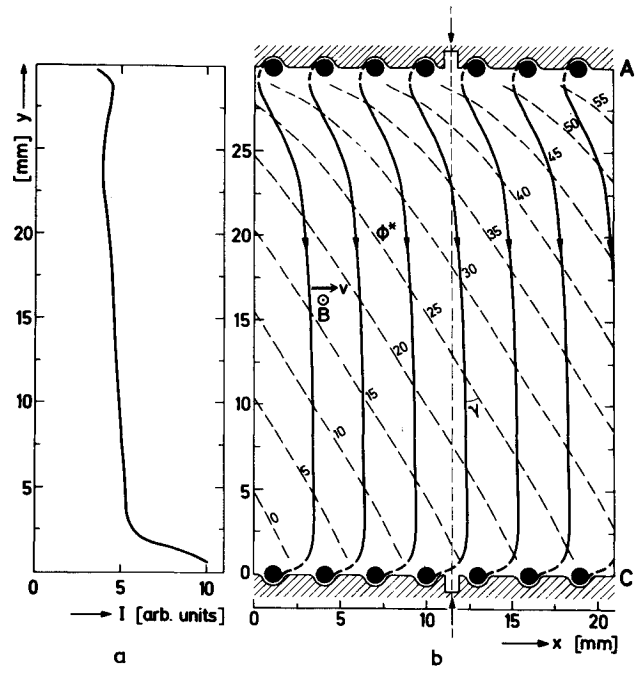

Fig. 5 Intensity distribution of the potassium resonance lines along the dotted line in Fig. 5b (a); time averaged distributions of the equipotential lines ϕ = const and current streamlines (b). $s/h = 0.1$; $B = 4.5$ tesla; $T_g = 2000°K$; $p = 1.3$ bar; $V = 420$ mps; $\langle j \rangle = 6$ amp/cm^2, short-circuit conditions.

here and, moreover, $\langle E_y \rangle$ involves a high degree of uncertainty. For this reason only the curve of the $\langle \beta \rangle$-value calculated in this magnetic field range is plotted in Fig. 4c. It can, however, be regarded as experimentally certain that β_{app} passes through a maximum in the range $0.3 \leqq B \leqq 0.7$ tesla that lies between the values $1.8 \leqq \beta_{app} \leqq 2.6$. For $B > 1.3$ tesla β_{app} then attains a saturation value whose upper and lower bounds corresponding to the lower and upper bounds of the sum of the cathode and anode drops are plotted in Fig. 4c.

In Fig. 4a the short-circuit current densities calculated with Eqs. (1–26) (Sec. 2) are also plotted ($\beta_{eff} = 1.5$ assumed). For U_E[Eq. (25)] the mean values of the experimental values given in Fig. 3 were used and σ_{eff} was determined with Eqs. (16, 17, and 24). A detailed comparison between the experimental and theoretical values will not be made, however, till Sec. 5.3, in which the current-voltage characteristics are treated.

Equation (3b) was used to calculate the effective Hall parameter from the β_{app} values given in Fig. 4c. The β_{eff} values in Fig. 4c agree within the experimental accuracy with the values obtained in Ref. 18 under similar conditions and also with the values theoretically predicted for ionization instabilities.

In Fig. 4b the Hall field strength increases linearly with the magnetic field strength in the high induction range ($s/h = 0.1$). The same qualitative behavior was also obtained every time the segmentation ratio was reduced to $s/h = 0.06$. In this case the Hall field strength inside the duct increased to a value of $\langle E_x \rangle = 28$ v/cm at $B = 5$ tesla for a $v \times B$ induced current flux, and to $\langle E_x \rangle = 58$ v/cm when the current flux was increased by applying additional external electric fields to the individual electrode pairs. In no case was either saturation or breakdown of the Hall voltage observed.

The linear rise of the Hall voltage ($B > 1.3$ tesla) with the magnetic induction as well as the fact that the measurements yield the theoretically predicted saturation value for the effective Hall parameter (Fig. 4c), and that periodic conditions prevailed up to the end of the duct (Fig. 2) indicate that neither boundary layers, which, as described in Ref. 6, lead to internal short-circuits, nor leakage currents due to inadequate insulation occur. In order, however, to confirm this by direct measurements and establish the extent of the current line bulging, the current distribution in the generator duct was determined.

First the intensity distribution (Fig. 5a) of the potassium resonance doublets between two electrode pairs in the y-direction along the dashed line in Fig. 5b was measured. This intensity is a measure of the electron temperature, which in turn is a measure of the absolute value of the current density as long as relaxation effects do not impair the Saha equilibrium between T_e and N_e. Such a deviation can, however, practically be ruled out here since periodic conditions prevail in the test region.

The curve in Fig. 5a shows that the current densities present on the cathode wall side at the insulator section have to be much higher than in the center of the duct. On the anode side, on the other hand, only a slight increase is observed. From these results it can be concluded that the current near the cathode wall has a nonnegligible j_x component, which must cause bulging of the streamlines inside the duct. The amount of bulging was found by determining the time averaged current direction from the time averaged equipotential distribution. This was measured in the region of seven electrode pairs with a movable electrostatic probe. The necessary vB values were determined under open-circuit conditions. The previously measured value of $\beta_{eff} = 1.5$ was used for determining the current direction. The resulting current distribution is plotted in Fig. 5b with one streamline per electrode pair. From this figure it can be seen that the current component in the x direction is very small inside the duct. In the immediate vicinity of the wall it was not possible to determine the potential distribution and hence the current direction either. From the streamline distribution inside the duct it follows, however, that a current must flow in the direction of the wall. Owing to relaxation effects[28] this current is higher on the cathode side than on the anode side. Both current components should be considered responsible for the intensity maxima in Fig. 5a.

5.3 Current Voltage Characteristics

After the performance of the generator had been investigated under open and short-circuit conditions all the electrode pairs of the generator were loaded with various resistances (2.5 Ω, 4.7 Ω, 10.3 Ω, 23 Ω for $s/h = 0.06$ and 0.1; 1.6 Ω, 3.1 Ω, 6.8 Ω, 16 Ω for $s/h = 0.2$). The voltage drop U_L at the resistance and the current I_y flowing through it were then measured at magnetic inductions of $B = 3$, 4, and 5 tesla. In Fig. 6a–c, such current voltage characteristics are shown. The experimental data provided with the margin of error were averaged over 6 pairs of electrodes (Nos. 23, 25, 27, 29, 31, 33). These average values do not differ very much from the values of the individual electrode pairs in the region considered.

In order to get a better understanding of the performance of the generator, the current-voltage characteristics were also calculated for the various cases measured. Allowance was thereby made for the influence of the finite segmentation of the electrodes and the fact that in a "nonequilibrium generator" the current paths are elongated compared with an "equilibrium generator," which results in a higher internal resistance. The voltage drop at the electrodes, the radiation losses and the reduction of the electrical conductivity and Hall parameter by the ionization instability were also taken into account (for details see Sec. 4). Leakage currents did not need to be considered here because the measurements already made under the more extreme conditions of the short-circuit case revealed the absence of such currents.

In Sec. 4 four different formulas for the effective electrical conductivity were proposed [Eqs. (16, 17, 23, 24)]. However, formula (23) was not investigated any further because of the uncertainty in the value of β_{eff}. In Fig. 6b these three relations are evaluated, whereas in Fig. 6a and 6c only Eq. (24) has been used. In all cases an average value was taken for the voltage drop at the electrodes. From Fig. 6b it can be seen that formula (17) produces the most favorable characteristic, much better than the experimental data. However, the case is different with the relations (16) and (24); both fit the measurements reasonably well, (24) a little bit better than (16), and so we have taken only Eq. (24) in Fig. 6a and 6c.

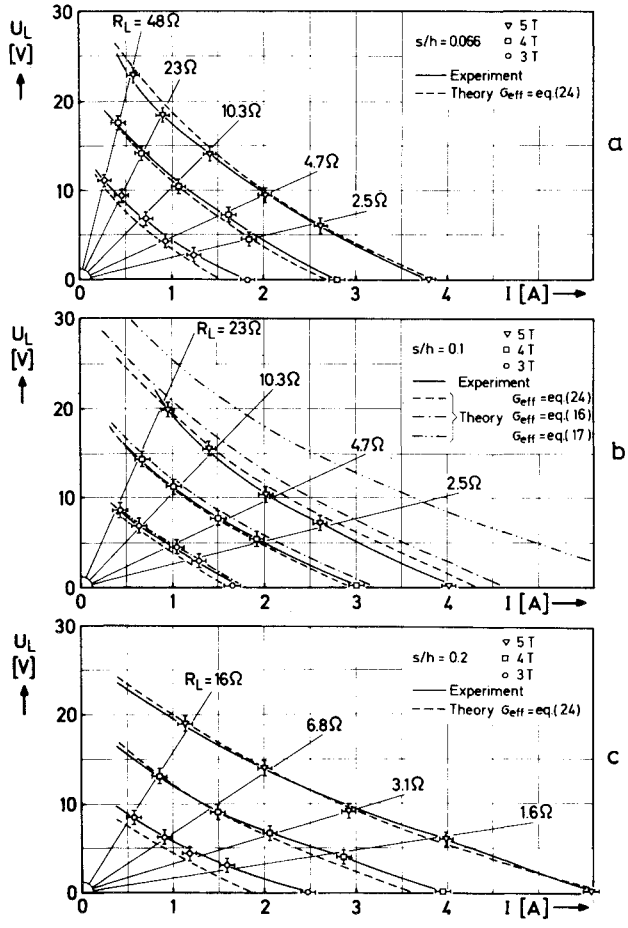

Fig. 6 Current-voltage characteristics at segmentation ratios s/h = 0.06 (a); 0.1 (b); 0.2 (c) (theory and experimental values). B = 3, 4, and 5 tesla; T_g = 2000 K; p = 1.29, 1.33, 1.30 bar; V = 420, 412, 425 mps.

It must now be asked whether this good agreement between theory [Eqs. (16) and (24)] and experiment is accidental or not and how far it may serve to judge the accuracy of our theoretical model as regards the generator performance. No striking systematic deviations could be observed in the region investigated, where the parameters s/h, B and the load resistances R_L were varied over wide ranges. However, in the calculation there are some quantities which have to be taken from measurements, and which are known only within a certain accuracy. In this context the most important quantities are V, T_g, p, B, U_E, and c. The margins of error connected with these quantities will here be given in terms of correction factors K defined as the ratio of the possible value and the reference value of a quantity, e.g., for the gas velocity $K_v = V/V_{ref}$. For V, c, and U_E the K-factors are expected to be in the range $0.95 \leqq K_{V,c,U_E} \leqq 1.05$, and for T_g, p and B in the range $0.97 \leqq K_{T_g,p,B} \leqq 1.03$. These possible errors give the theoretically calculated characteristics a certain bandwidth. Its magnitude and its dependence on the various experimental parameters can be most conveniently demonstrated by investigating the change of the short-circuit current density keeping all the experimental parameters constant but one. Figure 7 presents the results of such calculations whereby the following reference values have been used: B = 5 tesla, V = 412 m/s, T_g = 2000°K, p = 1.33 bar, c = 0.14% K, U_E = 15.6 V, and I_y = 4.5 A. Only the curves corresponding to a change in T_g, p, and c have been omitted because they are less important and less pronounced. Outside the margins of error the curves are drawn as broken lines. According to these calculations the short-circuit current density is extremely sensitive to even very small changes in the gas velocity V.

Because of the bandwidth of the characteristics caused by the uncertainty of the experimental values entering the calculations it has to be checked in what range the system of equations describing the generator performance has to be changed in order to make the characteristics fit the experimental data, in our special case the point $K_{v,B,U_E} = 1$. There are two possibilities of "fiddling with the knobs." As was already pointed out in Sec. 4, the expression $\sigma_{eff}/(1+g\beta_{eff})$, which can be considered as a measure of the internal resistance of the generator, involves uncertainty regarding the magnitude of the factor g. The second uncertainty is due to the dependence of the effective electrical conductivity on the magnetic field or which of the formulas for σ_{eff} should be taken. Corrections to the theory can be made only in these two points. In order to get an idea of the magnitude of the bandwidth caused by variations in g and σ_{eff} we introduce new correction factors $C_g = g/g_{ref}$, $C_{\sigma I} = (\sigma_{eff}/\sigma_{eff}^{ref})_{II}$, $C_{\sigma II} = (\sigma_{eff}/\sigma_{eff}^{ref})_{II}$, $C_{\sigma III} = (\sigma_{eff}/\sigma_{eff}^{ref})_{III}$. g_{ref} is given by 1.4 s/h [Eq. (6a)]. The reference values, I, II, and III of the various effective electrical conductivities can be obtained from the relations (16, 17, and 24). The short-circuit current density was now calculated by varying only one C factor and keeping all the others constant and equal to unity. It can be seen in Fig. 7 that the variation of σ_{eff} exerts the stronger influence on the short-circuit current density. The curves presented in Fig. 7 now give us opportunity to make an estimate of the range in which the C_g and $C_{\sigma I,\sigma II,\sigma III}$ factors are allowed to move.

As a consequence of the uncertainty in determining the gas velocity ($0.95 \leqq K_v \leqq 1.05$) the deviations between the measured and calculated values of the short-circuit current density are expected to be in the range $0.85 \leqq K_I \leqq 1.16$. However, the theory can be made to fit the experimental data by changing the value of one of the factors C_g and C_σ or both of them simultaneously. The range of variation is biggest if only one factor is varied. In the case of $0.95 \leqq K_v \leqq 1.05$ one obtains $0.66 \leqq C_g \leqq 1.36$, $0.88 \leqq C_{\sigma I} \leqq 1.04$, $0.68 \leqq C_{\sigma II} \leqq 0.88$, $0.91 \leqq C_{\sigma III} \leqq 1.08$.

As the other experimental values also contain errors, the range of variation of the C values can be even wider, viz., when these errors add. This case is, however, very unlikely since the large number of experimental values makes partial compensation more likely. If it is now assumed that the experimental values are in the middle of the error margin so that the probability that the actual values coincide is greatest, and if not only the short-circuit current density but also the entire characteristics are considered, the following ranges of fluctuation of the C values can be regarded as realistic: $0.7 \leqq C_g \leqq 1.3$; $0.85 \leqq C_{\sigma I} \leqq 1.05$ and $0.9 \leqq C_{\sigma III} \leqq 1.1$. The values obtained from the relation (17) ($C_{\sigma II}$) are no longer taken into account here since they deviated too strongly from the experimental values in the entire range. It should also be noted here that it is not possible to derive from the measurements which of the formulas (16) and (24) best

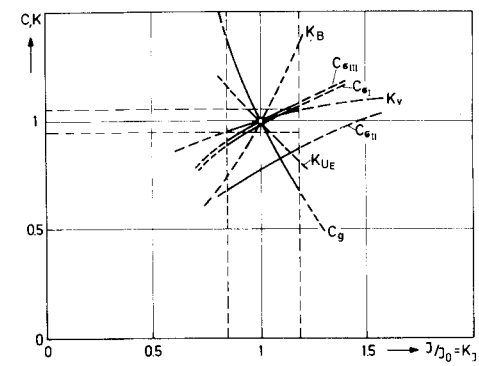

Fig. 7 Effect of parameter variations on the short-circuit current density (reference values s/h = 0.1; B = 5 tesla; T_g = 2000°K; p = 1.33 bar; V = 412 mps; U_E = 15.6 V).

describes the generator performance, and so both of them can be used on an equal footing for the generator calculation.

Regarding Eq. (16) this result is surprising since the discharge structure in the generator is governed not only by the ionization instabilities, but also by the streamers, i.e., it is more complicated than the model used for deriving Eq. (16). From the agreement between the theoretical and experimental results it is therefore reasonable to conclude that the streamers practically do not impair the generator behavior.

What has been said on the calculations of the generator performance should not be allowed to create the impression that the scaling laws for the calculation of a commercial subsonic generator have already been determined. In order to obtain reliable information, it is first necessary to make investigations with larger generator dimensions in which not only the cross-sectional area but also the generator length, which should be a multiple of the interaction length $L_p = p/\sigma_{\text{eff}} vB^2$, have to be increased. In this connection it might also be checked whether the relation $\sigma_{\text{eff}}/(1+g\beta_{\text{eff}})$ always correctly describes the internal resistance of the generator. Furthermore, σ_{eff} should also be investigated at higher pressures and also in the case of a He-Cs mixture.

Finally, the power density actually converted in the generator was determined from the behavior of the measured characteristics and the respective voltage drops at the electrodes. For this purpose that part of the electric energy dissipated in the anode and cathode drops had to be added to that dissipated in the load resistances. With a segmentation ratio of $s/h = 0.06$ a maximum power density of $N = 40$ mw/m^3 was obtained for a load factor of $K_{\text{eff}} = (U_L + U_E)/vBh = 0.25$. For higher factors of $K_{\text{eff}} = 0.5$ and $K_{\text{eff}} = 0.6$, which are better approximations for practical requirements, the power densities achieved were $N = 20$ and 15 mw/m^3, respectively. With higher segmentation ratios the power densities were correspondingly lower.

6. Conclusions

The investigations of the generator performance yielded the following results:

1) The prerequisite for effective generator operation is good insulation of the duct so that leakage currents cannot flow either in the direction of the induced $v \times B$ e.m.f. or in the Hall direction.

2) When these conditions were satisfied the open-circuit voltage showed the expected linear increase with rising magnetic induction in the range up to 5 tesla. The open-circuit voltage was higher than would be in keeping with the mean flow velocity. This is accounted for by the velocity profile, which was measured with a pitot tube, and can be regarded as proof that there are practically no short-circuit currents in the plasma. Measurements of the open-circuit voltage are suitable as a simple quality check on the insulation of the generator duct.

3) The short-circuit current density as a function of the magnetic induction showed the behavior expected in the presence of ionization instabilities. The same applies to the Hall voltage. Saturation phenomena were not observed in this case although it was possible with an additional increase of the current flux by external electric fields to attain maximum Hall field strengths of 58 v/cm inside the duct.

4) The voltage drops at the electrodes depended only on the electrode current and not on the magnetic induction.

5) From the equipotential distribution it was concluded that the current streamlines bulge only slightly downstream.

6) Comparison of the measured and calculated current-voltage characteristics showed that the generator performance in the parameter range investigated is correctly described by the system of Eqs. (1–26) (Sec. 4) together with one of the relations for the effective electrical conductivity

$$\frac{\sigma_{\text{eff}}}{\langle\sigma\rangle} = \left(\frac{\sigma_N{}^2 + \beta_{\text{crit}}{}^2}{\sigma_N{}^2 + \langle\beta\rangle^2}\right)^{1/2} \quad (16) \quad \text{or} \quad \frac{\sigma_{\text{eff}}}{\langle\sigma\rangle} = \frac{\beta_{\text{crit}}}{\langle\beta\rangle} \quad (24)$$

7) This result, however, does not necessarily allow the conclusion (Sec. 5.3) that the Eqs. (1–26) can also be applied to generators which have larger dimensions or are operated with supersonic flow. Furthermore, it has to be checked, whether relations (16) and (24) always correctly describe the effective electrical conductivity in a higher pressure range and also in the case of a plasma with a different composition (Ar-Cs or He-Cs).

In general, it can be stated that the investigations conducted here have shown that it is possible to build a subsonic generator which has neither leakage currents due to inadequate insulation nor internal short-circuits in the plasma, and which can therefore operate, in principle, as theoretically predicted.

References

[1] Zauderer, B. and Tate, E., "Electrode Effects and Gas Dynamic Characteristics of a Large Non-Equilibrium MHD Generator with Cesium Seeded Noble Gases," *12th Symposium on Engineering Aspects of MHD*, Argonne, Ill., 1972, pp. 1.6.1–10.

[2] Malikov, M. M., "Faraday Type MHD Channel with Essentially Non-Equilibrium Plasma," *Fifth International Conference on MHD Electrical Power Generation*, Vol. II, Munich, April 19–23, 1971, pp. 371–386.

[3] Bohn, Th., Grawatsch, K., Holzapfel, C., Komarek, P., Lang, H., and Noak, G., "Measurements with ARGAS II," *Fifth International Conference on MHD Electrical Power Generation*, Vol. II, Munich, April 19–23, 1971, pp. 403–413.

[4] Sovie, R. J. and Nichols, L. D., "Results of Initial Subsonic Tests in the NASA-LEWIS Closed Loop MHD Generator," *11th Symposium on Engineering Aspects of MHD*, Pasadena, Calif., 1970, pp. 82–89.

[5] Gasparotto, M., Gay, P., Toschi, R., and Bertolini, E., "Constant Velocity Subsonic Experiments with Closed Cycle MHD Generator," *Fifth International Conference on MHD Electrical Power Generation*, Vol. II, Munich, April 19–23, 1971, pp. 415–425.

[6] Decker, R., Hoffmann, M. A., and Kerrebrock, J. L., "Behavior of a Large Nonequilibrium MHD Generator," *AIAA Journal*, Vol. 9, No. 3, March 1971, pp. 357–364.

[7] Hsu, M. S., Solbes, A., and Kerrebrock, J. L., "Performance of a Nonequilibrium MHD Generator with Slanted Electrode Walls," *12th Symposium on Engineering Aspects of MHD*, Argonne, Ill., March 27–29, 1972, pp. I.1.1–7.

[8] Brederlow, G., Borde, R., Hartmann, J., Geisreiter, C., and Witte, K. J., "Device for Operating a Closed Loop MHD Generator with Various Measuring Facilities," IPP Rept. IV/35, 1972, Max-Planck-Institut für Plasmaphysik, F.R. Germany.

[9] Riedmüller, W., Brederlow, G., and Salvat, M., "Über die Anwendbarkeit der Linienumkehrmethode zur Messung der Elektronentemperatur in einem schwach ionisierten Edelgas-Alkali-Plasma," *Zeitschrift für Naturforschung*, Vol. 23a, 1968, pp. 731–743.

[10] Burger, J. and Brederlow, G., "Measurements of the Current Directions and Field Fluctuations due to Ionisation Instabilities in a Simulated Faraday Type MHD Generator," *11th Symposium on Engineering Aspects of MHD*, Pasadena, Calif., 1970, pp. 203–208; also IPP Rept. 3/104, 1969, Max-Planck-Institut für Plasmaphysik, F.R. Germany.

[11] Riedmüller, W., "Experimental Investigation of Instabilities in a Potassium Seeded Argon Plasma in Crossed Electric and Magnetic Fields," *Fourth International Conference on MHD Electrical Power Generation*, Vol. I, Warsaw, July 1968, pp. 519–528.

[12] Salvat, M., "The Effect of the Electrode Geometry on the Currents and Potentials in MHD Generators," IPP Rept. 3/68, 1968, Max-Planck-Institut für Plasmaphysik, F.R. Germany.

[13] Fischer, F. W. and Celinski, Z. N., "Two Dimensional Analysis of MHD Generators," IPP Rept. 3/26, 1965, Max-Planck-Institut für Plasmaphysik, F.R. Germany.

[14] Lengyel, L. L., "Two-Dimensional Current Distribution in Faraday Type MHD Energy Converters Operating in the Non-equilibrium Conducting Mode," *Energy Conversion*, Vol. 9, 1969, pp. 12–13.

[15] Sutton, G. W. and Sherman, A., *Engineering Magnetohydrodynamics*, McGraw-Hill, New York, 1965, p. 162.

[16] Frost, L. S. and Phelps, A. V., "Momentum Transfer Cross Sections for Slow Electrons in He, Ar, Kr, and Xe from Transport Coefficients," *Physical Review*, Vol. 136A, 1964, pp. 1538–1545.

[17] Schwenn, R., Brederlow, G., and Salvat, M., "Electrical Conductivity of an Argon Potassium Plasma at Low Current Densities as a Function of the Gas Temperature," *Plasma Physics*, Vol. 10, 1968, pp. 1077–1099.

[18] Brederlow, G. and Hodgson, R. T., "Electrical Conductivity in Seeded Noble Gas Plasmas in Crossed Electric and Magnetic Fields," *AIAA Journal*, Vol. 6, No. 7, July 1968, pp. 1277–1284.

[19] Brode, R. B., *The Physical Review*, Vol. 34, 1929, pp. 673–678.

[20] Solbes, A., "Quasilinear Plane Wave Study of Electrothermal Instabilities," *Electricity from MHD*, Vol. I, 1968, pp. 499–518.

[21] Riedmüller, W., "The Effective Electrical Conductivity of a Non-equilibrium MHD Plasma," Rept. IPP IV/52, 1973, Max-Planck-Institut für Plasmaphysik, F.R. Germany.

[22] Feneberg, W., "The Electrical Conductivity of a Partially Ionized Argon Potassium Plasma in a Magnetic Field," Rept. IPP 6/51, 1966, Max-Planck-Institut für Plasmaphysik, F.R. Germany.

[23] Dykhne, A., "Anomalous Plasma Resistance in a Strong Magnetic Field," *Soviet Physics JETP*, Vol. 32, 1971, pp. 348–351.

[24] Nakamura, T., "An Investigation of the Electrothermal Instability with a Current Component Parallel to the Magnetic Field," PhD thesis, 1970, MIT, Cambridge, Mass.

[25] Brederlow, G. and Witte, K. J., "Effective Electrical Conductivity and Electron Temperature Measurements in a Non-Equilibrium MHD Generator Plasma at Atmospheric and Higher Pressure," *13th Symposium on Engineering Aspects of MHD*, Stanford, 1973, pp. I.7.1–I.7.6.

[26] Merck, W., "On the Fully Developed Turbulent Compressible Flow in an MHD Generator," Ph.D. thesis, 1971, TH Eindhoven.

[27] Brederlow, G., Lengyel, L. L., and Zinko, H., "Reduction of the Open Circuit Voltage by Boundary Layer Leakage Currents in Experimental Faraday Type MHD Generators," *4th International Conference on MHD Electrical Power Generation*, Vol. I, Warsaw, 1968, pp. 419–430.

[28] Dodel, G., "Experimental Investigation of Current Density Distributions in an Argon Potassium Plasma Streaming through a Channel with Segmented Electrodes," *Plasma Physics*, Vol. 12, 1970, pp. 273–292.

[29] Lengyel, L. L., "On Current and Potential Distributions in Non-equilibrium MHD Plasmas at High Magnetic Field Strength," *AIAA Journal*, Vol. 9, No. 10, Oct. 1971, pp. 1957–1962.